Global assessment of spatiotemporal changes of frequency of terrestrial wind speed

Yanan Zhao[1], Shijing Liang[1], Liu Yi[1], Tim R.McVicar[2], Cesar Azorin-Molina[3], Lihong Zhou[1], Robert J H Dunn[4], Sonia Jerez[5], Yingzuo Qin[1], Xinrong Yang[1], Jiayu Xu[1], Zhenzhong Zeng [1,*]

[1] School of Environmental Science and Engineering, Southern University of Science and Technology, Shenzhen, China

[2] CSIRO Land and Water, Black Mountain, Canberra, AC

[3] Centro de Investigaciones sobre Desertificación—Spanish National Research Council (CIDE, CSIC-UV-Generalitat Valenciana), Moncada (Valencia), Spain

[4] Met Office Hadley Centre, Exeter, United Kingdom

[5] Department of Physics, University of Murcia, Murcia, Spain

* Correspondence: zengzz@sustech.edu.cn (Z. Zeng)

Manuscript for *Environmental Research Letter*

January 18, 2022

Abstract:

Wind energy, an important component of clean energy, is highly dictated by the disposable wind speed within the working regime of wind turbines (typically between 3 - 25 m s^{-1} at the hub height). Following a continuous reduction ("stilling") of global annual mean surface wind speed (SWS) since the 1960s, recently, researchers have reported a "reversal" since 2011. However, little attention has been paid to the evolution of the effective wind speed for wind turbines. In this study, we used hourly *in-situ* observations to analyze the wind speed frequency variations at various wind speed ranges and quantify their contributions to the average SWS changes over 1981-2021. We found that during the stilling period (here 1981-2010), the frequency of strong SWS (>=5.0 m s^{-1}, the 80^{th} of global SWS) decreased with a rate of -1.83% $decade^{-1}$ ($p < 0.001$), contributing 212.20% to the continuous weakening of SWS. The frequency of slight SWS (0.1 m s^{-1} < SWS < 2.2 m s^{-1}) increased with a rate of 3.63% $decade^{-1}$ ($p < 0.001$), contributing 102.9% to offset the decline of mean SWS. During the reversal period of SWS (here, 2011-2021), nearly all SWS ranges defined here contributed to a strengthening of SWS. The strengthened strong wind (>= 5.0 m s^{-1}) contributed 80.2% to the trend change of SWS from decrease to increase in 2011. Based on the synthetic capacity factor series calculated by considering commercial wind turbines (General Electric GE 2.5-120 model with rated power 2.5 MW) at the locations of the meteorological stations, the frequency changes resulted in a reduction of wind power energy (-10.02 TWh yr^{-1}, $p < 0.001$) from 1981 to 2010 and relatively weak recovery (2.67 TWh yr^{-1}, $p < 0.05$) during 2011-2021.

Keywords: wind speed, frequency changes, wind energy, power curve, strong winds

1. Introduction

Wind energy is a key component of the energy market and a potential way for climate mitigation (IEA, 2020). In 2021, the global wind industry reached 94 GW power capacity addition, mainly driven by China, Europe and the United States. Yet, the current installation rates suggest that it will still be challenging to meet the 1.5℃ mitigation goal (Council G W E, 2022). To promote wind energy expansion, understanding the efficiency of wind power generation is necessary. Wind power generation is particularly sensitive to changes in wind speed as wind power is proportional to the cubic of wind speed (McElroy *et al* 2009, Pryor *et al* 2020, Eurek *et al* 2017, Sohoni *et al* 2016). Global annual mean near-surface wind speed (SWS) continuously declined over the past five decades before 2010, known as the period of "stilling" (Roderick *et al* 2007, Vautard *et al* 2010, McVicar *et al* 2012), with a decrease rate of -0.08 m s^{-1} $decade^{-1}$ during 1978-2010 (Zeng *et al* 2019). But during the past ten years (i.e., 2011 - ~2017), such stilling phenomenon has been replaced by a "reversal", with an increasing annual mean SWS of 0.24 m s^{-1} $decade^{-1}$ since (Zeng *et al* 2019). Regionally, consistently increasing mean SWS has been confirmed in South Korea (Kim and Paik 2015), China (Li *et al* 2018, Liu *et al* 2022), Saudi Arabia (Azorin-Molina *et al* 2018), Spain and Portugal (Utrabo *et al* 2022) and Sweden (Minola *et al* 2022).

However, mean values of SWS are less likely to realistically reflect the wind power generation, because only the effective wind speed (typically between 3 - 25 m/s at the hub height) can be used in wind power generation. When winds are too light, they can't rotate the turbine blades, while strong winds force wind turbines to shut down to prevent damage (Lydia *et al* 2014). Moreover, due to the non-linear relationship between wind speed and power output, 90% of wind power production is from the upper half of the wind speed probability distribution and up to 25% of electricity is generated by the top 10% of wind speed (Pryor *et al* 2020). Therefore, beyond exploring the changes in mean annual SWS, investigating the change of SWS in different frequencies is more important for the energy sector.

Several researchers studied the variation of SWS frequency within different ranges: Vautard *et al* (2010) found a decreasing trend of strong wind frequency in the northern mid-

latitudes (1979-2008) by calculating the frequency of SWS exceeding a given incrementing threshold (i.e., 1 m s^{-1}, 3 m s^{-1}, …, 13 m s^{-1}, 15 m s^{-1}). Zha *et al* (2017) found a fast decline trend of strong wind frequency in China during 1970-2011. They classified the SWS in China based on the criteria of the China Meteorological Administration (CMA, 2003). The segmentations of the wind speeds used in these studies do not consider the right-skewed characteristics of the wind speed distribution (Jung and Schindler *et al* 2019). Additionally and critically, these studies address the change in SWS coinciding with the period of stilling (~1970 - ~2010), and the time span should be extended to include the recent reversal period (here ~2011 - 2021).

To fill these gaps, here we use the hourly SWS data from HadISD (Dunn *et al* 2014, 2016) to derive global and continental wind speed trends, aiming to set the stage for a comprehensive analysis of SWS frequency change in a period spanning from 1981 to 2021. SWS was divided into nine ranges (see details in section 2.2) to analyze the year-to-year SWS frequency variations and quantify the influence on the annual average SWS. We also used the power law to extrapolate the SWS to the wind speed at the hub height of a commercial wind turbine to do a power assessment and evaluate the effect of SWS frequency changes on wind power generation. Our research aims to draw more attention to the variation of wind speed frequencies and provides a new perspective for better evaluating the association between wind speed changes and wind energy production.

2. Data and methods

2.1 Dataset

We use the hourly SWS data provided by the Hadley Centre Integrated Surface Database (HadISD, Dunn *et al* 2014, 2016), which is a sub-set of the station data from the Integrated Surface Database (ISD, Smith *et al* 2011). These data were subject to a series of quality control procedures, including duplicate checks, neighbor outliers and distribution gap checks, to eliminate bad data and maintain data continuity (Dunn *et al* 2016). The HadISD has been used for the annual monitoring of wind in the Bulletin of the America Meteorological Society State in recent years (Dunn *et al* 2016), and has been widely used in previous studies (Woolway *et al* 2019, Millstein *et al* 2022, Zhou *et al* 2021). However, in the ISD, calm periods had been

erroneously replaced by missing data due to encoding issues; this mainly occurred in Asia and Europe (Figure 1c, Dunn *et al*, 2022a). HadISD version v.3.3.0.202201p and later implemented a simple correction for this issue, and so recovered many of the calm wind (SWS = 0 m s^{-1}) observations (for full details see Dunn *et al* 2022a). Thus, the versions earlier than version v.3.3.0.202201p, omitting many calm wind observations, may cause biased results in SWS analysis (Dunn *et al* 2022a). To verify the recovery of calm wind in HadISD, we derived the hourly SWS data (observed at 10 m above ground level) during 1981-2021 both from the earlier version, taken v.3.1.2.202107p as an example (9278 stations), and the later corrected version v3.3.0.2202202p (9555 stations). We later analyzed the difference in calm wind frequency derived from the earlier data and corrected data (see section 3.1).

2.2 Methods

(a) Homogenization and resample of SWS data

To ensure the continuity of the long-term decadal analysis of SWS frequency, we implemented strict selection criteria for SWS time series to use a final subset of qualified stations. The final subset of stations is required to meet the following standards: (1) each final station needs to have continuous monthly records over 1981-2021; (2) each month should have more than 15 days of records; (3) the daily values must have at least four observations. After the data selection process, the final subset of stations includes 1,513 and 1,511 stations in version (v.3.1.2.202107p) and version (v3.3.0.202202p), respectively (see Figure 1c for station locations).

To obtain the frequency of SWS, we resampled the time series data to address the issue that the observations have inconstant observation intervals. According to Appendix Figures A1 and A2, the average intervals for all the stations in one year varies from 8h to 1h, and some stations have a shorter observation interval since 1990; the standard deviation of the observation intervals is greater than 1 for about 40% of the station, implying the inconstant observations in one year. Uneven observation intervals add noise signals when calculating wind speed frequencies on the annual scale, as observations with shorter time intervals tend to be more frequent. Therefore, it becomes necessary to transform SWS into equally time-spaced data.

Here, we fill the time gap by repeating the previous value in the time gap. For example, if the time interval is n hours (1 < n <= 48), there will be n - 1 hours without records, which will be filled by the value before this time gap. Even with continuously selected stations, there still exists dozens of hours between observations for some sites since we selected stations with records larger than 15 days per month. If the observation interval, n, is greater than 48 hours, the gap won't be filled because the value before the gap is no longer representative of such a long time period. The biases caused by this resampling method will be discussed in Section 3.2.

(b) Wind speed classification criteria

Cut-in and cut-out wind speeds are considered to decide the classification criteria for categorizing the SWS in power generation. The cut-in wind speed denoted as v_i', refers to the minimum wind speed that results in the turbine commencing rotating and generating electricity. The cut-out wind speed, marked as v_f', is the maximum wind speed to generate usable power. The cut-in and cut-out wind speeds refer to the wind speed at the hub height of the wind turbine. Here we use the parameters of the General Electric GE 2.5-120 wind turbine model with v_i' of 3.0 m s^{-1} and v_f' of 25.0 m s^{-1} (https://en.wind-turbine-models.com/turbines/310-ge-general-electric-ge-2.5-120).

The exponential wind profile power-law relation is applied to transform v_i' and v_f' at 110 m height from the 10-m wind speed records. The power-law relationship can be expressed as follows:

$$u_{tb} = u_s\left(\frac{z_{tb}}{z_s}\right)^{\alpha} \quad (1)$$

where u_{tb} and u_s represent wind speed at height z_{tb} (110 m) and z_s (10 m), and α is a nondimensional parameter usually assumed to be constant 1/7, which is broadly applicable to low surface roughness and adopted by some studies involving wind power assessment (Liu *et al* 2019, Islam *et al* 2011, Wang *et al* 2016). The cut-in (v_i) and cut-out (v_f) wind speeds at 10 m above the ground surface transformed from the wind profile power law are 2.2 m s^{-1} and 17.7 m s^{-1}.

Thus, the classification criteria of SWS are based on two aspects: (1) the cut-in and cut-out wind speeds defining the range of efficient SWS used in power generation; (2) the incrementing percentiles of SWS among efficient SWS. The incrementing percentiles refer to the average values of 50th, 60th, 70th, 80th, and 90th of the SWS over the 41 years and over all stations globally, which corresponds to the 2.8 m s^{-1}, 3.4 m s^{-1}, 4.1 m s^{-1}, 5.0 m s^{-1}, and 6.2 m s^{-1}. At the same time, we consider zero SWS into one separate group to verify the result of data correction (Dunn *et al* 2022a) and describe small wind speeds more accurately. Then SWS data was divided into nine ranges to show the changes in the SWS frequency at different ranges (Table 1). We denote SWS in specific range *i* as class *i* (*i*=1,2…9, Table 1). Here, SWS of class 3-8 is efficient wind speed.

(c) Quantification of the influence of the SWS frequency variation

To validate the categorization, we use the Pearson correlation coefficient to compare the SWS from *in-situ* data and weighted-average speed calculated by the following formula:

$$Weighted_v(t) = \sum_{i=1}^{9} \overline{v}_i f_i(t) \quad (2)$$

where $\overline{v}$ is the climatological mean of SWS of the corresponding wind speed category over 41 years (all the subscripts indicated the wind speed range), $Weighted_v(t)$ and $f_i(t)$ are the wind speed and frequency of year *t* accordingly.

To estimate the contribution of SWS frequency changes of each class to the wind speed trend, we keep the frequency of a specific class of SWS to be a constant value (the climatology mean value over 41 years) to calculate the fixed weighted-average SWS. The fixed weighted-average SWS ($Fixed_v$) of class k is computed as below:

$$Fixed_{v_k}(t) = \sum_{i=1}^{9} \overline{v}_i f_i(t) - \overline{v}_k f_k(t) + \frac{1}{41}\sum_{t=1}^{41} \overline{v}_k f_k(t) \quad (3)$$

The difference ($Diff_v$) between the weighted-average speed ($Weighted_v$) and fixed weighted-average SWS ($Fixed_v$) represented as formula (4) reflect the influence of a specific range of SWS to the average wind speed trend:

$$Diff_{v_k}(t) = Weighted_v(t) - Fixed_{v_k}(t) = \overline{v}_k f_k(t) - \frac{1}{41}\sum_{t=1}^{41} \overline{v}_k f_k(t) \quad (4)$$

Since $Weighted_v$ is proved to reconstruct the observed average SWS trend in section 3.2, we use $Weighted_v$ to replace observed SWS when quantifying the contributions of changes in wind speed frequencies to changes in mean SWS. The contributions can be calculated by the ratio of the trend of $Diff_v$ to the trend of $Weighted_v$ based on least square error linear regression.

(d) Wind power assessment

The theoretical power assessment of wind turbines requires complex parameters such as wind direction, air density and turbine parameters, which introduces vast complexity to set influencing parameters properly (Sohoni *et al* 2016), especially when considering the global spatial extent of our study. The power curve of wind turbines is helpful for wind energy forecasting without further technical details of wind power operating conditions (Lydia *et al* 2014). It is widely used in wind power assessment (Millstein *et al* 2022, Wang *et al* 2016, Pryor *et al* 2020). Here we estimate the wind energy that can be generated using the General Electric GE 2.5-120 wind turbine model (2.5 MW, 120 m diameter, and hub height at 110 m and 139 m) following Zeng *et al*.'s work (2019). We assume the wind turbine GE 2.5 – 120 was installed around each observation site and use its power curve to derive the wind power output under the wind regime at observation sites. Wind turbines at higher hub heights tend to have better wind regimes with stronger wind and generate more energy (Yang *et al* 2018). In this research, we considered hub heights of 110 m and 139 m to ensure that the results are comprehensive and convincing. Yearly wind power generation ($Energy$, Unit: GW·h) is calculated by combining the global wind turbine installations and the capacity factor based on formula (5), that is, the ratio of wind power output (P_{real}, Unit: MW) to rated power (P_{rated} = 2.5 MW) multiplied by the installed capacity (Unit: GW). Installed capacity data is from the Global Wind Energy Council (Council G W E 2022).

$$Energy = Capacity \times \frac{P_{real}}{P_{rated}} \times 365 \times 24 \quad (5)$$

(e) Trend analysis by piecewise linear regression

To quantify potential turning points in a specific time series, a piecewise linear regression model is applied to the time series of global annual SWS and wind power assessment (Toms

and Lesperance 2003, Ryan 2007). The piecewise linear regression model with a turning point (TP) can be described as follows:

$$y = \begin{cases} \beta_0 + \beta_1 t + \varepsilon, & t < \text{TP} \\ \beta_0 + \beta_1 t + \beta_2 (t - TP) + \varepsilon, & t \geq \text{TP} \end{cases} \quad (6)$$

where t is the year, β_0, β_1 and β_2 are regression coefficients, and ε is the residual of regression. The slope of the linear trend is β_1 before the TP (year) and $\beta_1 + \beta_2$ after the TP. Piecewise linear regression model optimizes the linear fitting parameters with the least sum of square error, which is capable of finding a turning point in a long-term time series, for instance, from a decreasing trend to an increasing trend, or from a significantly strengthening trend to a weak strengthening trend. T-test and Mann-Kendall trend test were used to detect the significance of the turning point and parameters in the piecewise linear fitting model (Wilks *et al* 2011). This method has been widely used in trend analysis (e.g., Zeng *et al* 2019, Yang *et al* 2021).

3. Results and discussion

3.1 Wind speed changes before and after data correction

Due to the missing calm wind in observations in previous HadISD versions, using SWS data from these HadISD versions overrates the wind speed reversal after 2013 (Dunn *et al* 2022a). Here we validated the effect of corrections to the calm wind missing in the updated HadISD (v3.3.0.202202p). Figure 1a-b shows the frequency change of calm wind in selected stations before and after data correction. Around 308 stations suddenly had no calm wind records after 2013 (Figure 1a). These stations mainly distribute in Asia and Europe (Figure 1c). After the data correction, the calm wind in problematic station data was replenished (Figure 1b). Hence, we adopt hereafter the latest version to do the analysis. In addition, numerous Chinese stations showed a decrease in the frequency of calm wind speed around 2004 (Figure 1a, Figure 6a). This is likely a direct benefit from the large-scale automation of meteorological stations implemented in China during 2004-05 (Zhang and Wang 2020), as continuous automatic observations are more likely to capture SWS change in the breeze in comparison to manual temporally sparse observations (e.g., once every 3-hours).

< Figure 1 here please >

We found that global SWS in the corrected HadISD showed a continuous decline during 1980-2010 with a rate of -0.08 m s^{-1} $decade^{-1}$ ($p < 0.001$). The turning year was near 2011, and then SWS increased at a rate of 0.096 m s^{-1} $decade^{-1}$ ($p < 0.001$, Figure 2a). At the continental scale, the changes in SWS from 1980 to around 2010 varied. In North America, Europe and Asia, a turning point marking the declining trend transferring to an increasing trend can be identified (Figure 2b-d). The declining SWS trends in America and Europe were close, with -0.118 m s^{-1} $decade^{-1}$ and -0.112 m s^{-1} $decade^{-1}$ (both $p < 0.001$), respectively, from 1980 to 2010. The slowing down of SWS was faster in Asia, with a trend of -0.136 m s^{-1} $decade^{-1}$ ($p < 0.001$). Moreover, the turning point indicating the wind speed reversal occurred early in 2000 in Asia, for example, in southwestern China (Yang *et al* 2012). While in Europe and North America, the turning points occurred later in 2013 and 2011, respectively. From 2011 to 2021, the reversed increasing trends of SWS in North America, and Europe were not significant, being respectively 0.084 m s^{-1} $decade^{-1}$ ($p > 0.05$), 0.056 m s^{-1} $decade^{-1}$ ($p > 0.05$), while the trend in Asia is 0.091 m s^{-1} $decade^{-1}$ ($p < 0.001$). The asymmetry between the SWS weakening trend and the SWS reversal trend is consistent with the previous studies (Wu *et al* 2018, Zeng *et al* 2019, Deng *et al* 2021; Liu *et al* 2022). Exploring the trends of SWS aids in the comprehensive analysis of SWS frequency variation.

< Figure 2 here please >

On the other hand, SWS in South America, Africa, and Australia did not show the first weakening and then reversing trend. In South America (Figure 2e) and Australia (Figure 2g), SWS presented continuous strengthening trends at a rate of 0.115 m s^{-1} $decade^{-1}$ and 0.225 m s^{-1} $decade^{-1}$ during 1981-2021, respectively. Yet, neither an increase nor decrease trend of SWS is found in Africa ($p > 0.05$, Figure 2f). The discrepancies in SWS trends in South America, Africa and Australia may be due to a lack of sufficient contiguous observations in these regions in the HadISD. For instance, the increasing trend of SWS was found in Australia based on the observations from 14 stations during 1975-2006 (Troccoli *et al* 2012). Meanwhile, a decreasing trend of SWS is found using observations from 163 stations for the same period (McVicar *et al* 2008). In addition, by analyzing eight reanalysis datasets, land SWS in the Southern

Hemisphere shows an increasing trend during 1982 - 2010 and a slightly decreasing trend later during 2010-2019 (Deng *et al* 2021). The SWS trend in the Southern Hemisphere remains highly uncertain, and more *in-situ* observation will help promote future research about SWS.

3.2 Frequency changes of global and regional SWS

Wind speed trends are closely associated with frequency. We found that the wind speed distribution had changed during the past decades (Figure 3a), implying the frequency change at different SWS categories. The peak of the wind speed distribution ranged from1.0-3.0 m s^{-1}, which has generally increased since 1981, implying an increase in the kurtosis of the curve. Moreover, the peak of the wind speed distribution shifts towards smaller values as time goes on (Figure 3a), implying an increase in the skewness in SWS frequency. A similar increase of skewness and kurtosis of SWS distribution was found during 2006–2019, as was predicted in 2020-2099 under the representative concentration pathway RCP8.5 (Jung and Schindler *et al* 2019).

< Figure 3 here please >

To calculate the frequencies of SWS, we resampled observed SWS into a 1-hour time-space (see Methods), which induces underestimation in earlier years of global observed average SWS (Figure 3b). Such underestimation faded during the wind reversal period (2011-2021, Figure 3b) since the fulfilling records with shorter observation intervals (Appendix Figure A1). However, there was still bias in Asia and Africa due to the restrained observation improvement (Appendix Figure A2).

After the SWS resampling, resampled SWS was divided into nine ranges based on the right-skewed wind speed distribution and contribution to wind energy generation (see Methods). To validate the categorization of SWS, the weighted-average SWS calculated from formula (2) was compared with the observed mean SWS after resampling (Figure 3b). The Pearson correlation coefficient of weighted-average SWS and the observed average was 0.998 ($p < 0.01$; Appendix Figure A3). The similarity between the weighted-average SWS and observed SWS implied that the classification criteria of SWS categorization were rather satisfying. Notice, however, that

there was a slight deviation between the weighted-average SWS and the observed SWS. This was because we used the climatological mean value of SWS to multiply the changing frequency when calculating weighted-average SWS.

The change in SWS frequency during the past decades is shown in Figure 4. Calm wind frequency decreased (-2.61% decade^{-1}, $p < 0.001$) for the past 41 years (Figure 4a). An increase with a rate of 3.47% decade^{-1} ($p < 0.001$) was found in class 2 (0.1-2.1 m s^{-1}) wind frequency (Figure 4b). However, the class 2 wind was smaller than the cut-in wind speed and thus didn't contribute to the wind power generation. The frequency of class 9 (> 17.7 m s^{-1}) wind was so small that the decrease rate was only -0.01% decade^{-1} ($p < 0.001$). Up to 60% of wind speed records fall in class 3-8 that can be used for wind power generation (Figure 4c-h). Among them, SWS frequency at class 3 and class 5 increased at a rate of 0.18% decade^{-1} and 0.37% decade^{-1} (both $p < 0.001$, Figure 4c, e), while SWS frequency at class 7 and class 8 decreased at a rate of -0.80% decade^{-1} and -0.59% decade^{-1} (both $p < 0.001$, Figure 4g-h). The trends of frequency change in class 4 and class 6 were not significant, with large fluctuations. Given that the increase in wind speed frequency mainly occurred for relatively low winds, we suggest that the reversal of global SWS was attributed to the decreasing frequency of calm winds and the increasing frequency of light winds. However, light winds are generally smaller than v_i (2.2 m s^{-1}), which has a limited effect on promoting wind power generation (Pryor and Barthelmie 2010).

< Figure 4 here please >

The decreasing frequency of relatively strong wind is noteworthy because a majority of wind power generation depends on the strong SWS (Tian *et al* 2019). Yet, the frequency of strong winds is usually minor, for example the frequency of SWS at class 9 is even less than 0.5% during a year. To quantify the influence of the changing SWS frequency on wind speed trend, we combined the frequency with climatological mean SWS at each class. Regarding a significant turning point around 2011, the trend of $Diff_v$ is analyzed separately in 1981-2010 and 2011-2021. During 1981-2010, a substantial change is found in class 2, class 7, and class 8 (Figure 5a). The $Diff_v$ at class 2 had significantly increased at a rate of 5.81% m s^{-1} decade^{-1} ($p < 0.001$), meaning that the increase in class 2 wind contributes 102.88% to offset part of the

global wind stilling trend (Figure 5b, Table 2). Nevertheless, the $Diff_v$ at class 7 and class 8 decreased by -5.27% m s^{-1} $decade^{-1}$ and -6.36% m s^{-1} $decade^{-1}$ ($p < 0.001$), respectively, meaning that the decrease in class 7 and class 8 winds contributed 93.30% and 112.62% to the wind stilling (Figure 5b, Table 2). After 2011, $Diff_v$ significantly increased for class 2, class 3 and class 8 winds, contributing 26.43%, 30.08% and 23.82% to wind speed reversal. Here both SWS at class 3 and class 8 are effective wind speeds, thus beneficial to power generation. However, other classes of effective winds had relatively less contribution to wind speed reversal, namely 9.24%, 16.37% and 1.61% at class 5, 6 and 7, respectively. Since the strong winds of class 7 and class 8 had an apparent trend change from -11.63% m s^{-1} yr^{-1} ($p < 0.001$, 1981-2010) to an increased rate of 3.36% m s^{-1} yr^{-1} ($p < 0.001$, 2011-2020), they had the largest contribution (i.e., 79.46%) to the trend changes of average SWS from stilling state to reversal state. The substantial decrease of strong winds during 1981–2010 and slight increase with fluctuation during 2011–2021 concords with the results of Dunn *et al* (2022b). Here, the $Diff_v$ in Figure 5a is always zero because class 1 only contains calm wind, though the frequency of calms does show variations.

< Figure 5 here please >

Regionally, the calm wind frequency in Asia and South America decreased from over 25% to below 10% from 1990-2010 (Figure 6a). The decrease was smaller for Africa, Australia and Europe (Figure 6a). Calm wind frequency did not show a noticeable change in North America, instead having significant interannual variations (Appendix Figure A4). In Asia, most winds were found to be the light wind of class 2, and the frequency of class 2 wind reached over 50% in 2000-2021 (Figure 6b). Moderate winds, of class 4 and class 5, were more frequent in Europe than in other continents, and both classes experienced an increment of 2% from 1981-2021 (Figure 6d-e). Australia is an exception for the observed increasing frequency of strong wind at classes 6-8, yet this is obtained by only 26 stations (Figure 6f-h). As for the class 9 wind frequency, a consistent decrease is found in nearly all continents (Figure 6i). This rapid decrease in strong wind concords with a series of earlier regional studies conducted in America (Pryor *et al* 2007, 2009), China (Guo *et al* 2011, Zha *et al* 2017), Central Asia (Dunn *et al* 2022b), the United Kingdom (Earl *et al* 2013) and Spain and Portugal (Azorin-Molina *et al* 2016).

< Figure 6 here please >

3.3 Effect of wind speed frequency change on wind power potential

To understand the role of continuously decreasing strong winds in wind energy generation, we made the effort to quantify the above results in terms of wind power generation potential both at global and continental scales without consideration of the influence of technological improvement. Based on global wind power capacity in 2021 (837 GW) and the power curve of wind turbine GE 2.5-120 at 110 m hub height, the wind energy was estimated to have a continued decline with a rate of -10.02 TWh yr^{-1} ($p < 0.001$) during 1981-2010, and then a reversal with a rate of 2.67 TWh yr^{-1} ($p < 0.05$) during 2011 - 2021 (Figure 7c). Wind energy was generally larger than 100 TWh when the hub height was 139 m, with a decreasing trend of -10.36 TWh yr^{-1} ($p < 0.001$) during 1981 – 2010 and an increasing trend of 2.95 TWh yr^{-1} ($p < 0.05$) during 2011–2021 (Appendix Figure A6), which suggested that hub height has a little impact on trend changes of wind energy. The wind energy mentioned below is all based on hub height = 110 m. Compared to the reversal trend of SWS, the recovery of wind power is much slighter. Re-analysis data also report no noticeable changes in mean annual global wind energy generation (Jung *et al* 2019). Wind power's reversal trend is relatively weak due to the decline in strong wind frequency.

< Figure 7 here please >

The wind power changes are quite different from the trend of SWS in Europe and Africa. In Europe, while the average SWS increased during the past decade (i.e., 2011 to 2021), the wind power decreased at a rate of -1.20 TWh yr^{-1} during 1998-2021 ($p < 0.001$, Figure 8b). Wind power in Africa also decreased in the past decade with a rate of -0.11% TWh yr^{-1} ($p < 0.05$, Figure 8e). The decrease in wind power in Europe and Africa was caused by the large decrease in strong winds at classes 6-8 (Figure 6f-h). Tian *et al*. (2019) also reported a decline in wind power potential in half of the stations in Europe and Africa. Meanwhile, the increase in wind power after the turning point (i.e., 2008) was not as substantial as the reversal of SWS in Asia (Figure 8c) in the recent decade (i.e., 2008 to 2021). The decreasing rate of wind power in Asia was -5.03 TWh yr^{-1} ($p < 0.001$) before 2008, while the increasing rate was only 1.49 TWh

yr^{-1} ($p < 0.05$) during 2008 - 2021. North America had the same phenomenon with a significant decrease rate of -2.01 TWh yr^{-1} ($p < 0.001$) during 1981-2013 and a non-significant increase rate of 0.83 TWh yr^{-1} ($p > 0.05$). Studies have also shown a slow increase in average wind energy in China and the United States over the last decades (Jung *et al* 2019). In addition, Australia and South America still maintained increasing trends of wind power during 1981-2021 with a rate of 0.54% TWh yr^{-1} ($p < 0.001$) and 0.77% TWh yr^{-1} ($p < 0.001$, Figure 8d, f), which is caused by increasing strong wind frequency at classes 6-8 in Australia and increasing wind frequency at classes 5-6 (Figure 6e-h) in South America, respectively. The regional analysis further proved that the weakening of strong winds hinders the upward trajectory of the global wind energy industry.

< Figure 8 here please >

4. Conclusion

We conducted a global spatio-temporal analysis on the variation of SWS trend and SWS frequency in recent decades (i.e., 1981-2021) and evaluated its impact on wind power generation. Analysis of wind speed frequencies emphasized that the decrease of strong wind frequency (SWS > 5.0 m s^{-1}) is a dominant cause of wind stilling with a contribution of 212.20%. In comparison, the continuous increase of the light wind (0.1 m s^{-1}< SWS < 2.8 m s^{-1}) accompanying the decreasing calm wind mainly contributes 56.51% to wind speed reversal. However, the continuous increase in the frequency of light wind made a negligible contribution to wind power generation. Therefore, the rise in wind power potential was not as optimistic as subjectively estimated based on the reversal trend of average SWS. Global mean annual wind power potential only showed a slight increase at a rate of 2.67 TWh yr^{-1} ($p < 0.05$) from 2011-2021 (the 1981-2010 rate was -10.02 TWh yr^{-1}, $p < 0.001$) compared to the substantial reversal of mean SWS at 0.09 m s^{-1} $decade^{-1}$ ($p < 0.001$) over 2011-2021 (the 1981-2010 rate is -0.08 m s^{-1} $decade^{-1}$, $p < 0.001$) of mean SWS.

Several issues deserve further research. The cause(s) of the continuously decreasing strong wind is yet to be fully explored and understood. Further evaluation of the frequency changes in the Southern Hemisphere is needed based on quality-controlled data with reliable trends from

homogenized observational networks and reanalysis datasets to generate quality-controlled data from which reliable trends can be evaluated. Meanwhile, more detailed regional assessments of wind energy help quantify the impact of continuing strong wind declines and benefit investment decisions.

Supplemental Information

Appendix Figures A1-A6

Acknowledgements

This study was supported by the National Natural Science Foundation of China (grant no. 42071022) and the start-up fund provided by Southern University of Science and Technology (no. 29/Y01296122). C. A-M was supported by the IBER-STILLING (RTI2018-095749-A-I00, MCIU/AEI/FEDER,UE); VENTS (GVA-AICO/2021/023); the CSIC Interdisciplinary Thematic Platform (PTI) Clima (PTI-CLIMA); and the 2021 Leonardo Grant for Researchers and Cultural Creators, BBVA Foundation. All the specific country observational organizations who establish, maintain, and run observational networks are the fundamental to the global ISD and HadISD databases.

Data availability statement

The data that support the findings of this study are available upon request from the authors.

Author contributions

Zhenzhong Zeng: Conceptualization, Methodology **Yanan Zhao:** Methodology, Software, Writing – Draft **All other authors:** Writing – Review & Editing

Reference.

Azorin-Molina C, Guijarro J-A, McVicar T R, Vicente-Serrano S M, Chen D, Jerez S and Espírito-Santo F 2016 Trends of daily peak wind gusts in Spain and Portugal, 1961–2014 *J. Geophys. Res. Atmospheres* **121** 1059–78. Doi: 10.1002/2015JD024485

Azorin-Molina C, Rehman S, Guijarro J A, McVicar T R, Minola L, Chen D and Vicente-Serrano S M 2018 Recent trends in wind speed across Saudi Arabia, 1978–2013: a break in the stilling *Int. J. Climatol.* **38** e966–e984. Doi: 10.1002/joc.5423

China Meteorological Administration (CMA) 2003 *Ground Surface Meteorological Observation* (China Meteorological Press, Beijing) https://www.cma.gov.cn/en2014/

Council G W E 2022 *Global Wind Report 2022* (Global Wind Energy Council: Brussels, Belgium) https://gwec.net/global-wind-report-2022/

Deng K, Azorin-Molina C, Minola L, Zhang G and Chen D 2021 Global Near-Surface Wind Speed Changes over the Last Decades Revealed by Reanalyses and CMIP6 Model Simulations *J. Clim.* **34** 2219–34 Doi: 10.1175/JCLI-D-20-0310.1

Dunn R J H, Azorin-Molina C, Menne M J, Zeng Z, Casey N W and Shen C 2022a Reduction in reversal of global stilling arising from correction to encoding of calm periods *Environ. Res. Commun.* **4** 061003 Doi: 10.1088/2515-7620/ac770a

Dunn R J H, Willett K M, Morice C P and Parker D E 2014 Pairwise homogeneity assessment of HadISD *Clim. Past* **10** 1501–22 Doi: 10.5194/cp-10-1501-2014

Dunn R J H, Aldred F, Gobron N, Miller J B, Willett K M, Ades M, Adler R, Allan R P, Anderson J, Anneville O, et al 2022b Global Climate *Bull. Am. Meteorol. Soc.* **103** S11–142 Doi: 10.1175/BAMS-D-22-0092.1

Dunn R J H, Willett K M, Parker D E and Mitchell L 2016 Expanding HadISD: quality-controlled, sub-daily station data from 1931 *Geosci. Instrum. Methods Data Syst.* **5** 473–91 Doi: 10.5194/gi-5-473-2016

Earl N, Dorling S, Hewston R and Glasow R von 2013 1980–2010 Variability in U.K. Surface Wind Climate *J. Clim.* **26** 1172–91 Doi: 10.1175/JCLI-D-12-00026.1

Eurek K, Sullivan P, Gleason M, Hettinger D, Heimiller D and Lopez A 2017 An improved global wind resource estimate for integrated assessment models *Energy Econ.* **64** 552–

67 Doi: 10.1016/j.eneco.2016.11.015

Guo H, Xu M and Hu Q 2011 Changes in near-surface wind speed in China: 1969–2005 *Int. J. Climatol.* **31** 349–58 Doi: 10.1002/joc.2091

International Energy Agency(IEA) 2020 World Energy Outlook 2020 (*OECO Publishing*) https://www.iea.org/reports/world-energy-outlook-2020

Islam M R, Saidur R and Rahim N A 2011 Assessment of wind energy potentiality at Kudat and Labuan, Malaysia using Weibull distribution function *Energy* **36** 985–92 Doi: 10.1016/j.energy.2010.12.011

Jung C and Schindler D 2019 Changing wind speed distributions under future global climate *Energy Convers. Manag.* **198** 111841 Doi: 10.1016/j.enconman.2019.111841

Jung C, Taubert D and Schindler D 2019 The temporal variability of global wind energy – Long-term trends and inter-annual variability *Energy Convers. Manag.* **188** 462–72 Doi: 10.1016/j.enconman.2019.03.072

Kim J and Paik K 2015 Recent recovery of surface wind speed after decadal decrease: a focus on South Korea *Clim. Dyn.* **45** 1699–712 Doi: 10.1007/s00382-015-2546-9

Li Y, Chen Y, Li Z and Fang G 2018 Recent recovery of surface wind speed in northwest China *Int. J. Climatol.* **38** 4445–58 Doi: 10.1002/joc.5679

Liu F, Sun F, Liu W, Wang T, Wang H, Wang X and Lim W H 2019 On wind speed pattern and energy potential in China *Appl. Energy* **236** 867–76 Doi: 10.1016/j.apenergy.2018.12.056

Liu Y, Zeng Z, Xu R, Ziegler A D, Jerez S, Chen D, Azorin-Molina C, Zhou L, Yang X, Xu H, Li L, Dong L, Zhou F, Cao R, Liu J, Ye B, Kuang X and Yang X 2022 Increases in China's wind energy production from the recovery of wind speed since 2012 *Environ. Res. Lett.* **17** 114035 Doi: 10.1088/1748-9326/ac9cf4

Lydia M, Kumar S S, Selvakumar A I and Prem Kumar G E 2014 A comprehensive review on wind turbine power curve modeling techniques *Renew. Sustain. Energy Rev.* **30** 452–60 Doi: 10.1016/j.rser.2013.10.030

McElroy M B, Lu X, Nielsen C P and Wang Y 2009 Potential for Wind-Generated Electricity in China *Science* **325** 1378–80 Doi: 10.1126/science.1175706

McVicar T R, Van Niel T G, Li L T, Roderick M L, Rayner D P, Ricciardulli L and Donohue R

J 2008 Wind speed climatology and trends for Australia, 1975–2006: Capturing the stilling phenomenon and comparison with near-surface reanalysis output *Geophys. Res. Lett.* **35** Online: https://onlinelibrary.wiley.com/doi/abs/10.1029/2008GL035627

McVicar T R, Roderick M L, Donohue R J, Li L T, Van Niel T G, Thomas A, Grieser J, Jhajharia D, Himri Y, Mahowald N M, Mescherskaya A V, Kruger A C, Rehman S and Dinpashoh Y 2012 Global review and synthesis of trends in observed terrestrial near-surface wind speeds: Implications for evaporation *J. Hydrol.* **416–417** 182–205 Doi: 10.1016/j.jhydrol.2011.10.024

Millstein D, Bolinger M and Wiser R 2022 What can surface wind observations tell us about interannual variation in wind energy output? *Wind Energy* **25** 1142–50 Doi: 10.1002/we.2717

Minola L, Reese H, Lai H-W, Azorin-Molina C, Guijarro J A, Son S-W and Chen D 2022 Wind stilling-reversal across Sweden: The impact of land-use and large-scale atmospheric circulation changes *Int. J. Climatol.* **42** 1049–71 Doi: 10.1002/joc.7289

Pryor S C, Barthelmie R J, Bukovsky M S, Leung L R and Sakaguchi K 2020 Climate change impacts on wind power generation *Nat. Rev. Earth Environ.* **1** 627–43 Doi: 10.1016/j.rser.2009.07.028

Pryor S C, Barthelmie R J and Riley E S 2007 Historical evolution of wind climates in the USA *J. Phys. Conf. Ser.* **75** 012065 Doi: 10.1088/1742-6596/75/1/012065

Pryor S C, Barthelmie R J, Young D T, Takle E S, Arritt R W, Flory D, Gutowski Jr. W J, Nunes A and Roads J 2009 Wind speed trends over the contiguous United States *J. Geophys. Res. Atmospheres* **114** Doi: 10.1029/2008JD011416

Pryor S C and Barthelmie R J 2010 Climate change impacts on wind energy: A review *Renew. Sustain. Energy Rev.* **14** 430–7 Doi: 10.1016/j.rser.2009.07.028

Roderick M L, Rotstayn L D, Farquhar G D and Hobbins M T 2007 On the attribution of changing pan evaporation *Geophys. Res. Lett.* **34** Online: https://onlinelibrary.wiley.com/doi/abs/10.1029/2007GL031166

Ryan S E 2007 A Tutorial on the Piecewise Regression Approach Applied to Bedload Transport Data *(U.S. Department of Agriculture, Forest Service, Rocky Mountain Research Station)*

Smith A, Lott N and Vose R 2011 The Integrated Surface Database: Recent Developments and

Partnerships Bull. Am. Meteorol. Soc. 92 704–8 Doi: 10.1175/2011BAMS3015.1

Sohoni V, Gupta S C and Nema R K 2016 A Critical Review on Wind Turbine Power Curve Modelling Techniques and Their Applications in Wind Based Energy Systems *J. Energy* **2016** e8519785 Doi: 10.1155/2016/8519785

Tian Q, Huang G, Hu K and Niyogi D 2019 Observed and global climate model based changes in wind power potential over the Northern Hemisphere during 1979–2016 *Energy* **167** 1224–35 Doi: 10.1016/j.energy.2018.11.027

Toms J D and Lesperance M L 2003 Piecewise Regression: A Tool for Identifying Ecological Thresholds *Ecology* **84** 2034–41 Doi: 10.1890/02-0472

Troccoli A, Muller K, Coppin P, Davy R, Russell C and Hirsch A L 2012 Long-Term Wind Speed Trends over Australia *J. Clim.* **25** 170–83 Doi: 10.1175/2011JCLI4198.1

Utrabo-Carazo E, Azorin-Molina C, Serrano E, Aguilar E, Brunet M and Guijarro J A 2022 Wind stilling ceased in the Iberian Peninsula since the 2000s *Atmospheric Res.* **272** 106153 Doi: 10.1016/j.atmosres.2022.106153

Vautard R, Cattiaux J, Yiou P, Thépaut J-N and Ciais P 2010 Northern Hemisphere atmospheric stilling partly attributed to an increase in surface roughness *Nat. Geosci.* **3** 756–61 Doi: 10.1038/ngeo979

Wang J, Hu J and Ma K 2016 Wind speed probability distribution estimation and wind energy assessment *Renew. Sustain. Energy Rev.* **60** 881–99 Doi: 10.1016/j.rser.2016.01.057

Wilks, D. S. 2011 Statistical methods in the atmospheric sciences *Academic press* Vol. 100

Woolway R I, Merchant C J, Van Den Hoek J, Azorin-Molina C, Nõges P, Laas A, Mackay E B and Jones I D 2019 Northern Hemisphere Atmospheric Stilling Accelerates Lake Thermal Responses to a Warming World *Geophys. Res. Lett.* **46** 11983–92 Doi: 10.1029/2019GL082752

Wu J, Zha J, Zhao D and Yang Q 2018 Changes in terrestrial near-surface wind speed and their possible causes: an overview *Clim. Dyn.* **51** 2039–78 Doi: 10.1007/s00382-017-3997-y

Yang H, Chen J and Pang X 2018 Wind Turbine Optimization for Minimum Cost of Energy in Low Wind Speed Areas Considering Blade Length and Hub Height *Appl. Sci.* **8** 1202 Doi: 10.3390/app8071202

Yang Q, Li M, Zu Z and Ma Z 2021 Has the stilling of the surface wind speed ended in China? *Sci. China Earth Sci.* **64** 1036–49 Doi: 10.1007/s11430-020-9738-4

Yang X, Zongxing L, Qi F, Yuanqing H, Wenlin A, Wei Z, Weihong C, Tengfei Y, Yamin W and Theakstone W H 2012 The decreasing wind speed in southwestern China during 1969–2009, and possible causes *Quat. Int.* **263** 71–84 Doi: 10.1016/j.quaint.2012.02.020

Zeng Z, Ziegler A D, Searchinger T, Yang L, Chen A, Ju K, Piao S, Li L Z X, Ciais P, Chen D, Liu J, Azorin-Molina C, Chappell A, Medvigy D and Wood E F 2019 A reversal in global terrestrial stilling and its implications for wind energy production *Nat. Clim. Change* **9** 979–85 Doi: 10.1038/s41558-019-0622-6

Zha J, Wu J, Zhao D and Yang Q 2017 Changes of the probabilities in different ranges of near-surface wind speed in China during the period for 1970–2011 *J. Wind Eng. Ind. Aerodyn.* **169** 156–67 Doi: 10.1016/j.jweia.2017.07.019

Zhang Z and Wang K 2020 Stilling and Recovery of the Surface Wind Speed Based on Observation, Reanalysis, and Geostrophic Wind Theory over China from 1960 to 2017 *J. Clim.* **33** 3989–4008 Doi: 10.1175/JCLI-D-19-0281.1

Zhou L, Zeng Z, Azorin-Molina C, Liu Y, Wu J, Wang D, Li D, Ziegler A D and Dong L 2021 A Continuous Decline of Global Seasonal Wind Speed Range over Land since 1980 *J. Clim.* **34** 9443–61 Doi: 10.1175/JCLI-D-21-0112.1

Figure Legends

Figure 1. Yearly frequency of calm wind speed and distribution of stations. Yearly frequency of calm wind (SWS = 0 m s^{-1}) in selected stations before (a) and after (b) data correction. The red line in (a) is a mark of 2013. The frequency of calm wind at stations from ~300 to ~500 and from ~600 to ~800 in the y-axis shows recovery in (b). **c)** distribution of selected stations. The orange points represent the stations without records of calm wind after 2013. The blue points and orange points are a total of 1,511 stations used in this research.

Figure 2. Decadal variation of global and continental mean SWS. a) Global mean SWS trend during 1981-2021 (black dots and line). The red line is the piecewise linear regression ($p < 0.001$). The dashed lines (n=400) are the mean value of SWS of a random selection (40%) from global stations. The turning point of SWS is statistically indicated in 2011 in the piecewise linear regression model. **b-g**) continental mean SWS trend during 1981-2021, being North America, Europe, Asia, South America, Africa, and Australia, respectively. The red lines are piecewise linear regression in (b-d) and simple linear regression in (e-g).

Figure 3. **Distribution change of SWS frequency and comparison between observed mean SWS, mean SWS after resampling, and weighted-average SWS. a)** the waterfall plot of SWS density distribution is derived by calculating the annual SWS frequency of a continuous wind speed range from 0-15 m s^{-1}. The line plot for each year is derived from the kernel density estimation of the SWS histogram. The lines correspond to the frequency which is also shaded in blue and green for visualization. **b**) black line with solid dots represents observed global mean SWS changes, the dashed line represents mean SWS after resampling the time series to a refined 1-hour timestamp from observed data and the brown line represents weighted-average SWS.

Figure 4. Changes of frequencies in nine ranges of SWS. The frequencies denoted by the black dot are the average frequencies of SWS, which take into account all stations in a specific class.

Figure 5. The change of the difference ($Diff_v$) between weighted-average SWS ($Weighted_v$) and fixed weighted-average SWS ($Fixed_v$). a) The trend of $Diff_v$ in the nine wind speed classes. **b**) Rate of deviations ($Diff_v$) during 1981-2011 and 2011-2021. Positive (negative)

values indicate the specific classes of fixed weighted-average SWS increases (decreases). The star represents that the trend is significant with *p*-value < 0.05. The symbol "n.s." means the trend is not significant. Error bars show the standard error of the slope in simple linear regression.

Figure 6. Changes of frequency in the nine wind speed classes of SWS over six continents during 1981-2021. a-i) Each sub-part shows an SWS class in six continents. The colors in the figure represent the values of frequency, please pay attention to the different ranges in each color bar.

Figure 7. Power curve of wind turbine and changes of global average wind power potential. a) Assume wind turbine GE 2.5-110 was installed at every *in-situ* station to derive wind power output under the specific wind regime of the station. **b)** Power curve of wind turbine GE 2.5-110. **c**) Global wind power potential is denoted by block point. The dashed lines (n=400) are the mean value of SWS of a random selection (40%) from global stations. The turning point in the piecewise linear regression model of wind power also happened in 2011 (R^2 = 94%, p < 0.001). The trend before and after the turning point of wind power is shown in the inset, where the increasing trend after the turning point is at an incredibly low rate. The mean SWS shown by the brown line is in a comparison with the increase rate of the average power.

Figure 8. Wind power potential over six continents during 1981-2021. a-c) The red line is the piecewise linear regression fit (p < 0.05). Each grey line (n=400) is the interannual trend of wind power for a randomly selected subset (40%) of stations on each continent. **d-f)** For the southern hemisphere, only a single linear regression was used as there was no clear turning trend.

Figures

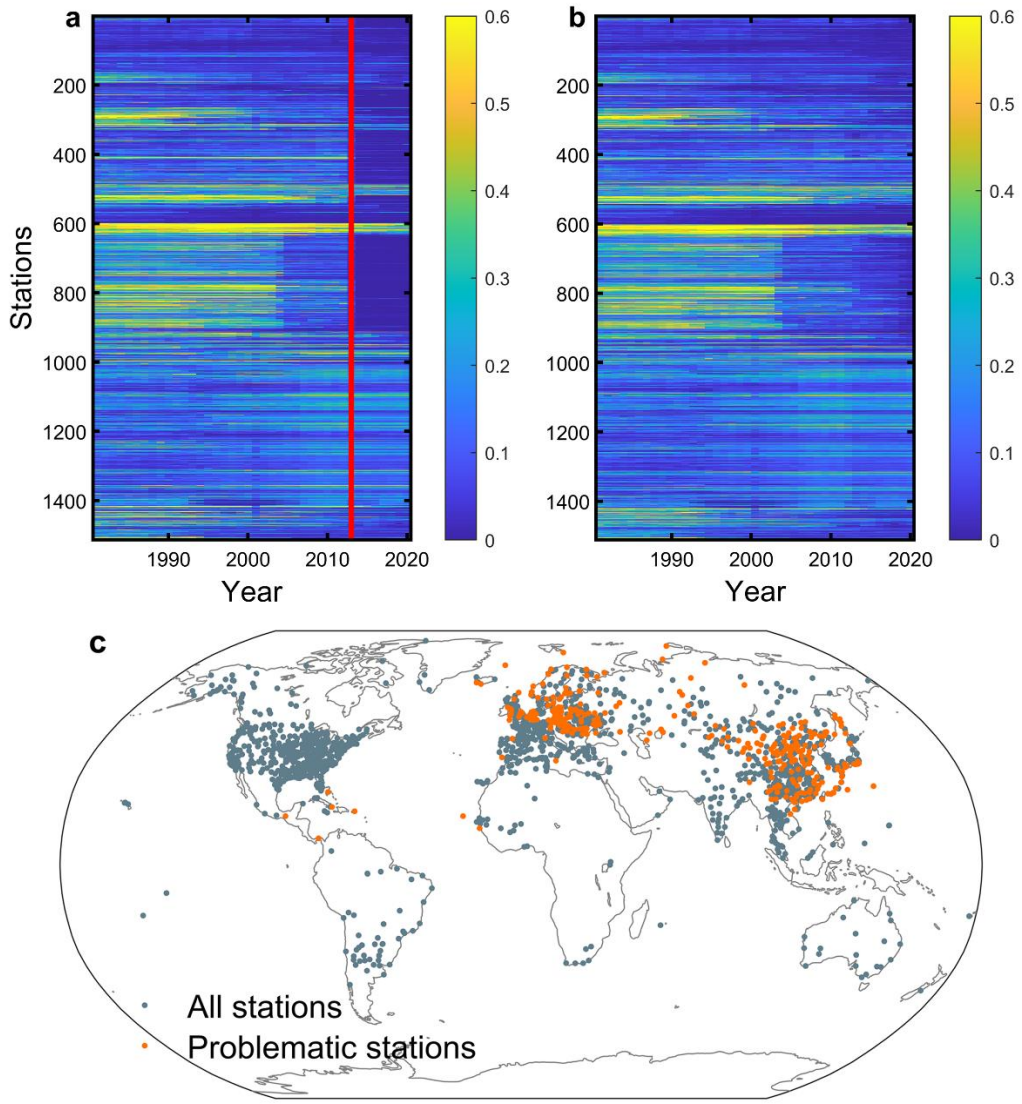

Figure 1. Yearly frequency of calm wind speed and distribution of stations. Yearly frequency of calm wind (SWS = 0 m s^{-1}) in selected stations before (a) and after (b) data correction. The red line in (a) is a mark of 2013. The frequency of calm wind at stations from ~300 to ~500 and from ~600 to ~800 in the y-axis shows recovery in (b). **c)** distribution of selected stations. The orange points represent the stations without records of calm wind after 2013. The blue points and orange points are a total of 1,511 stations used in this research.

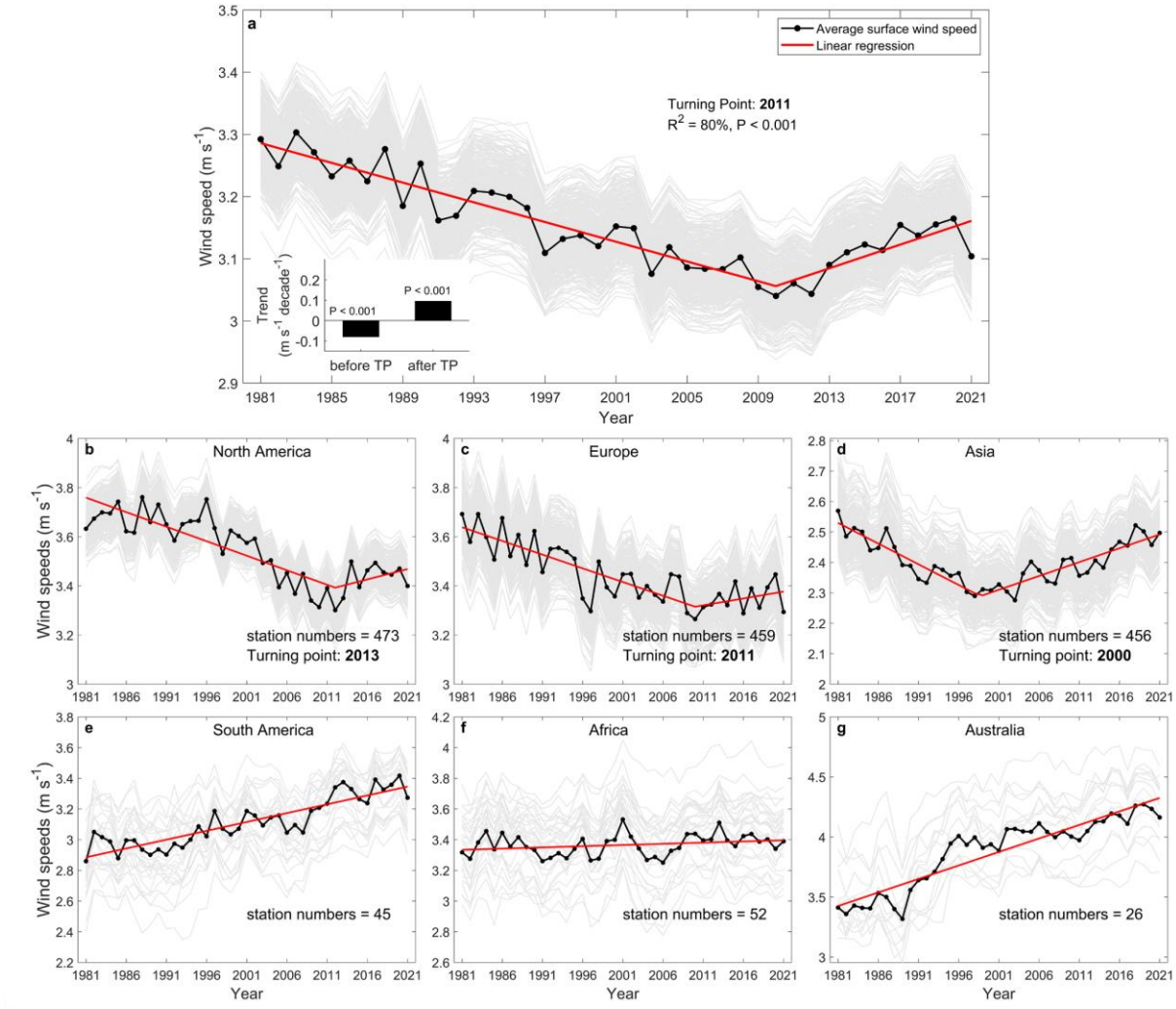

650

651 **Figure 2. Decadal variation of global and continental mean SWS. a**) Global mean SWS
652 trend during 1981-2021 (black dots and line). The red line is the piecewise linear regression (p
653 < 0.001). The dashed lines (n=400) are the mean value of SWS of a random selection (40%)
654 from global stations. The turning point of SWS is statistically indicated in 2011 in the piecewise
655 linear regression model. **b-g**) continental mean SWS trend during 1981-2021, being North
656 America, Europe, Asia, South America, Africa, and Australia, respectively. The red lines are
657 piecewise linear regression in (b-d) and simple linear regression in (e-g).

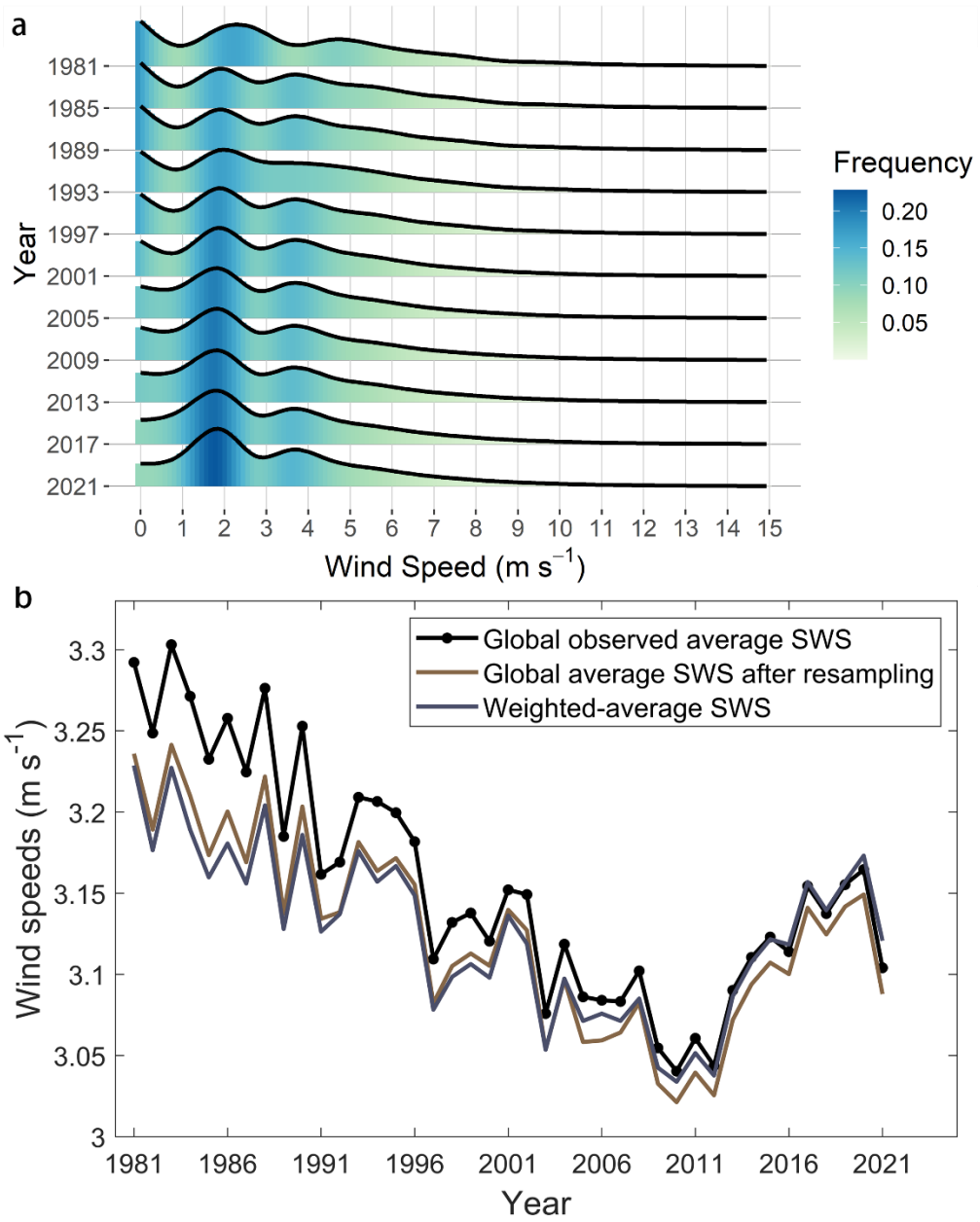

Figure 3. **Distribution change of SWS frequency and comparison between observed mean SWS, mean SWS after resampling, and weighted-average SWS. a)** the waterfall plot of SWS density distribution is derived by calculating the annual SWS frequency of a continuous wind speed range from 0-15 m s^{-1}. The line plot for each year is derived from the kernel density estimation of the SWS histogram. The lines correspond to the frequency which is also shaded in blue and green for visualization. **b**) black line with solid dots represents observed global mean SWS changes, the dashed line represents mean SWS after resampling the time series to a refined 1-hour timestamp from observed data and the brown line represents weighted-average SWS.

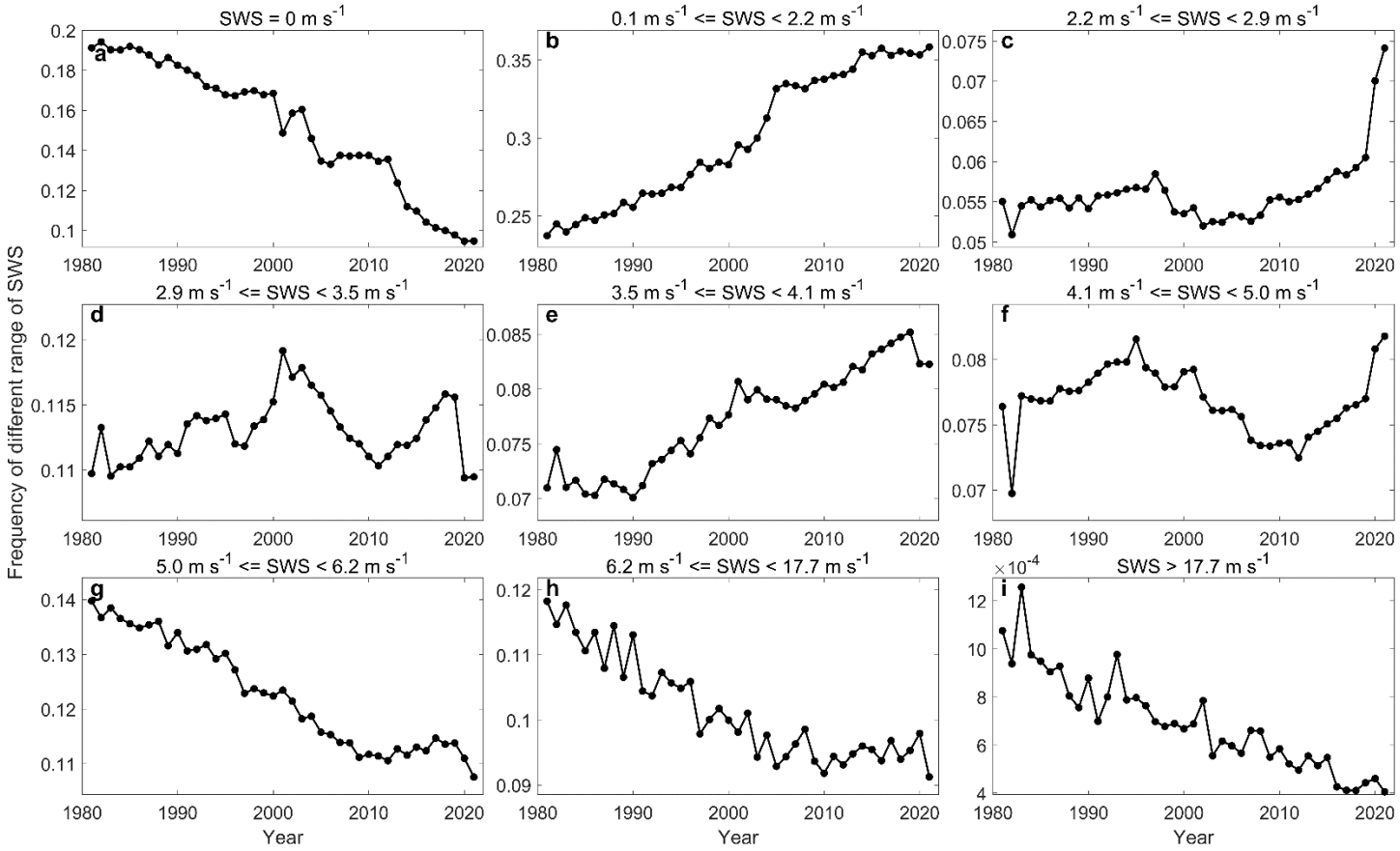

668

669 **Figure 4. Changes of frequencies in nine ranges of SWS.** The frequencies denoted by the black dot are the average frequencies of SWS, which

670 take into account all stations in a specific class.

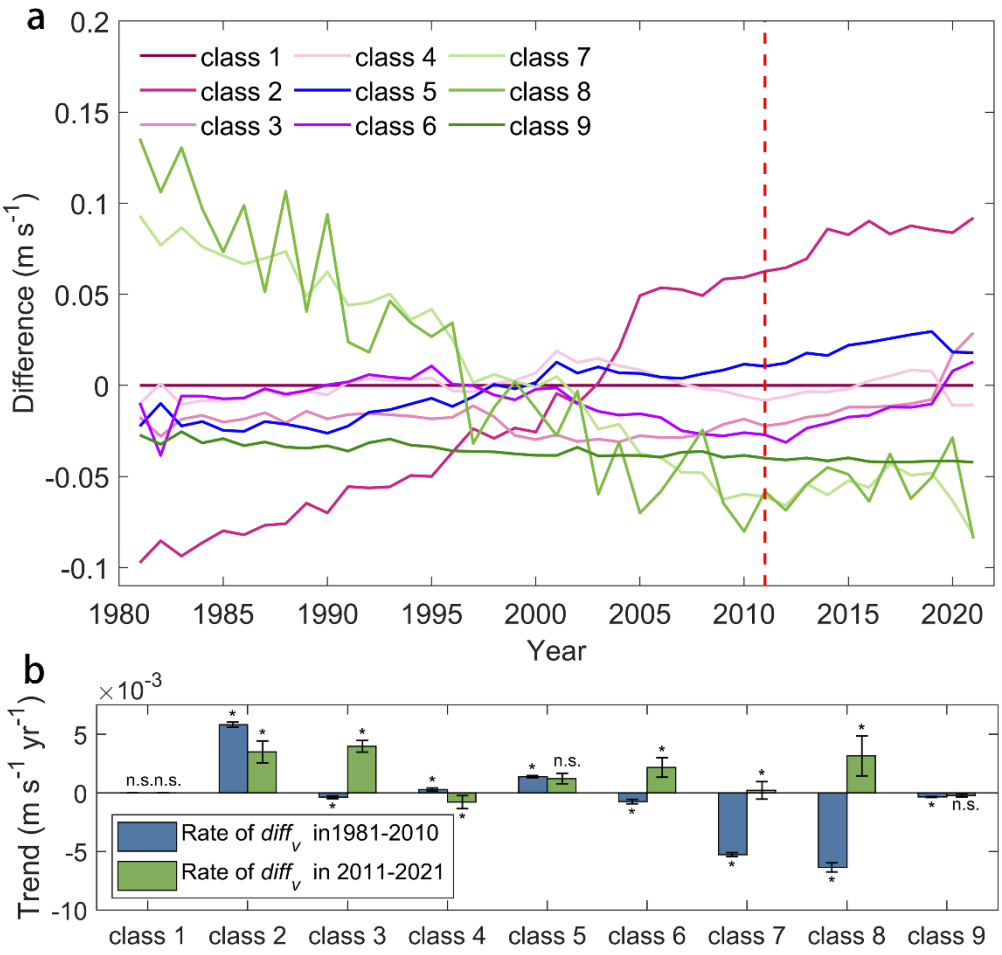

Figure 5. The change of the difference ($Diff_v$) between weighted-average SWS ($Weighted_v$) and fixed weighted-average SWS ($Fixed_v$). a) The trend of $Diff_v$ in the nine wind speed classes. **b**) Rate of deviations ($Diff_v$) during 1981-2011 and 2011-2021. Positive (negative) values indicate the specific classes of fixed weighted-average SWS increases (decreases). The star represents that the trend is significant with p-value < 0.05. The symbol "n.s." means the trend is not significant. Error bars show the standard error of the slope in simple linear regression.

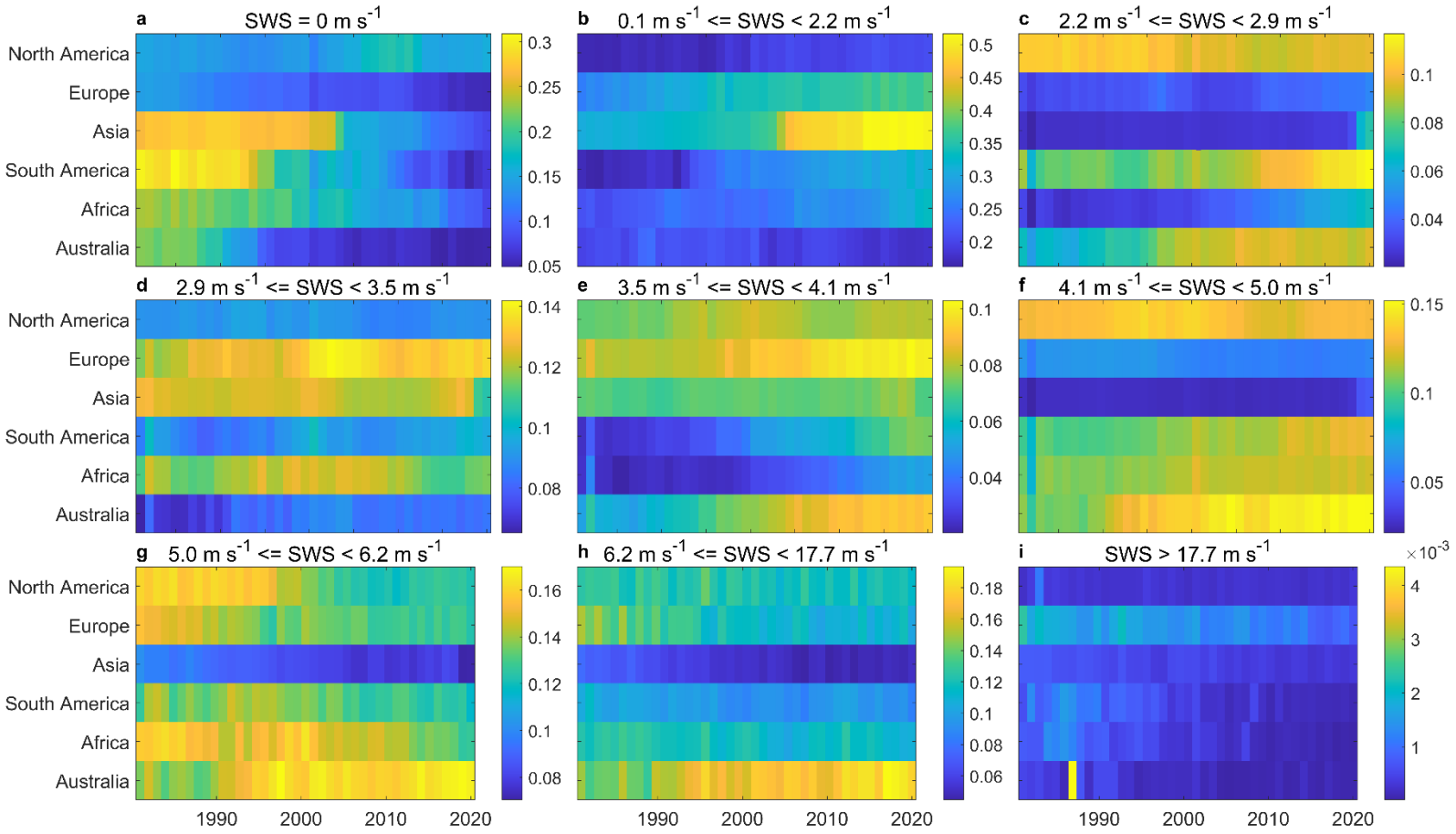

Figure 6. Changes of frequency in the nine wind speed classes of SWS over six continents during 1981-2021. a-i) Each sub-part shows an SWS class in six continents. The colors in the figure represent the values of frequency, please pay attention to the different ranges in each color bar.

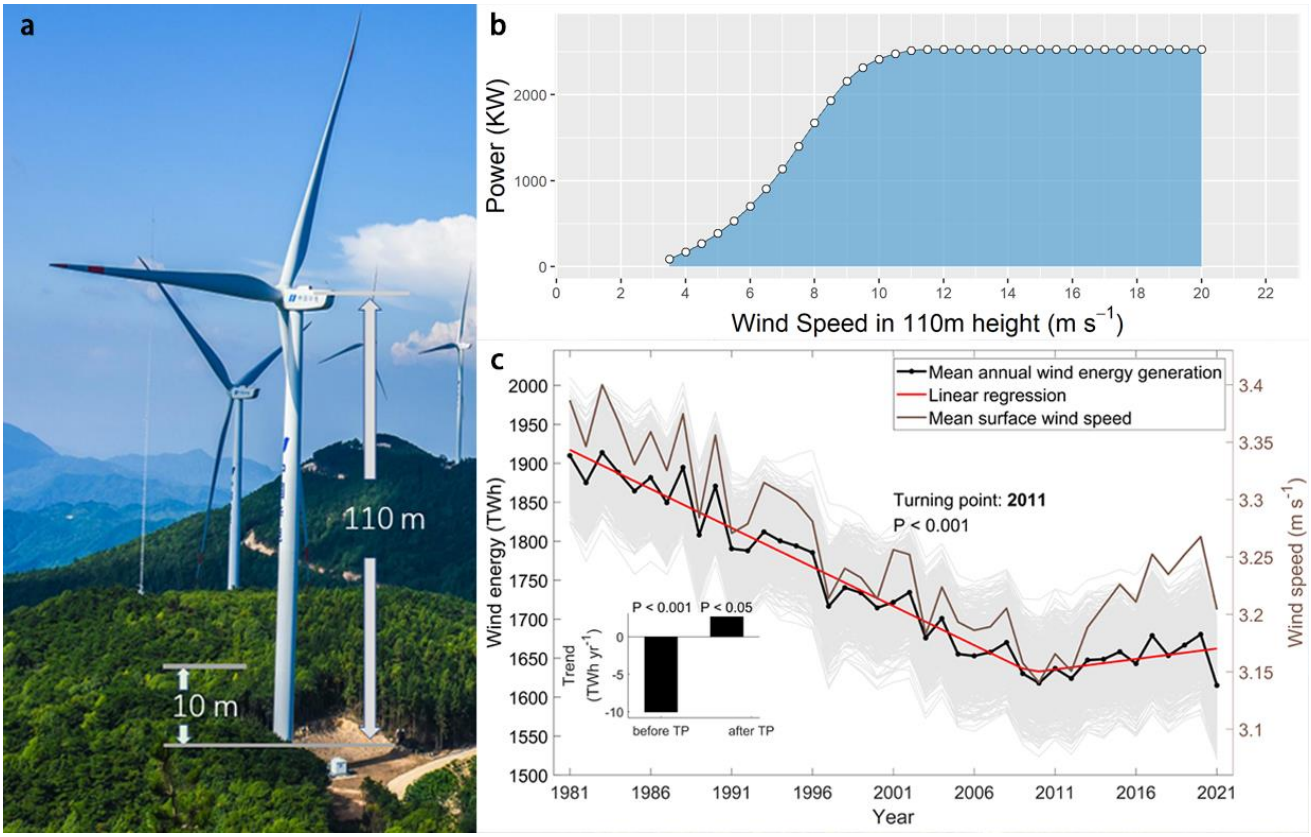

Figure 7. Power curve of wind turbine and changes of global average wind power potential. **a)** Assume wind turbine GE 2.5-110 was installed at every *in-situ* station to derive wind power output under the specific wind regime of the station. **b)** Power curve of wind turbine GE 2.5-110. **c**) Global wind power potential is denoted by block point. The dashed lines (n=400) are the mean value of SWS of a random selection (40%) from global stations. The turning point in the piecewise linear regression model of wind power also happened in 2011 (R^2 = 94%, p < 0.001). The trend before and after the turning point of wind power is shown in the inset, where the increasing trend after the turning point is at an incredibly low rate. The mean SWS shown by the brown line is in a comparison with the increase rate of the average power.

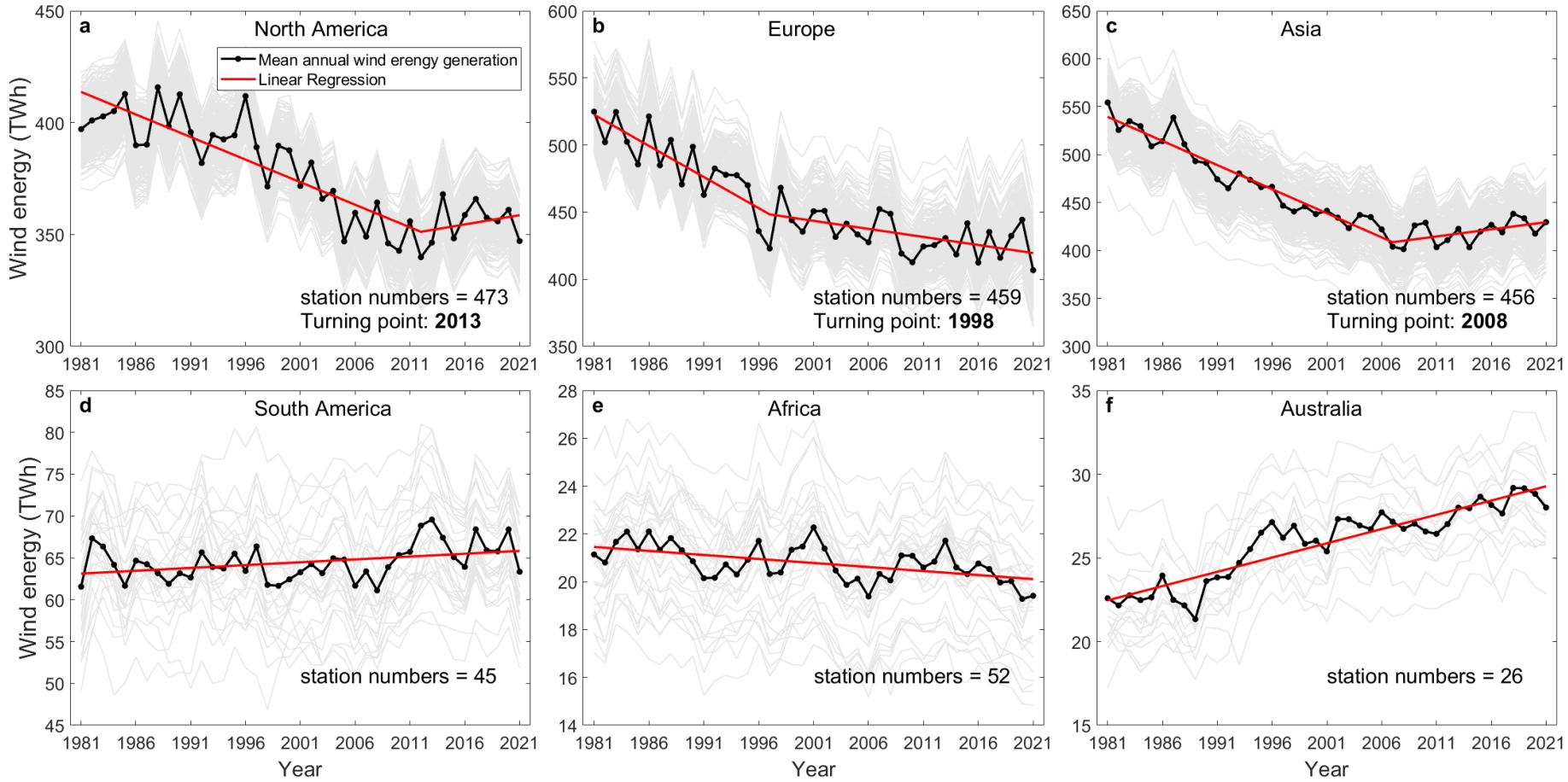

Figure 8. Wind power potential over six continents during 1981-2021. a-c) The red line is the piecewise linear regression fit ($p < 0.05$). Each grey line (n=400) is the interannual trend of wind power for a randomly selected subset (40%) of stations on each continent. **d-f)** For the southern hemisphere, only a single linear regression was used as there was no clear turning trend.

Appendix

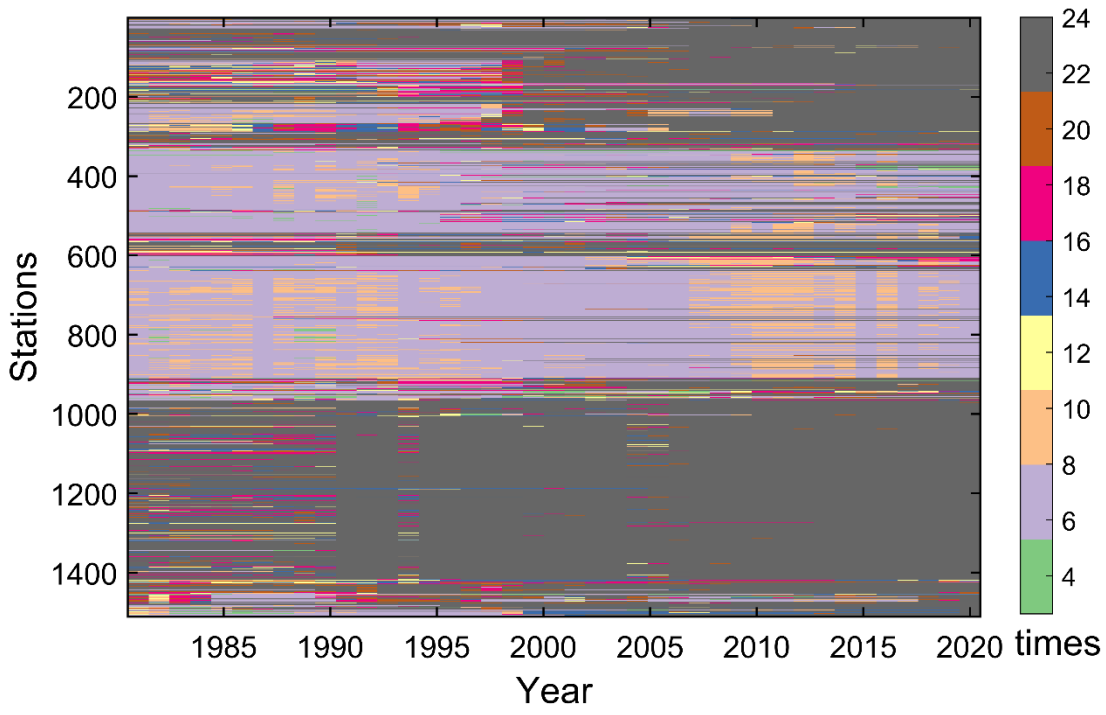

Appendix Figure A1. Average daily observation (reporting) times across stations and years. For example, the largest daily observation times is 24, meaning the recorded time interval is one hour.

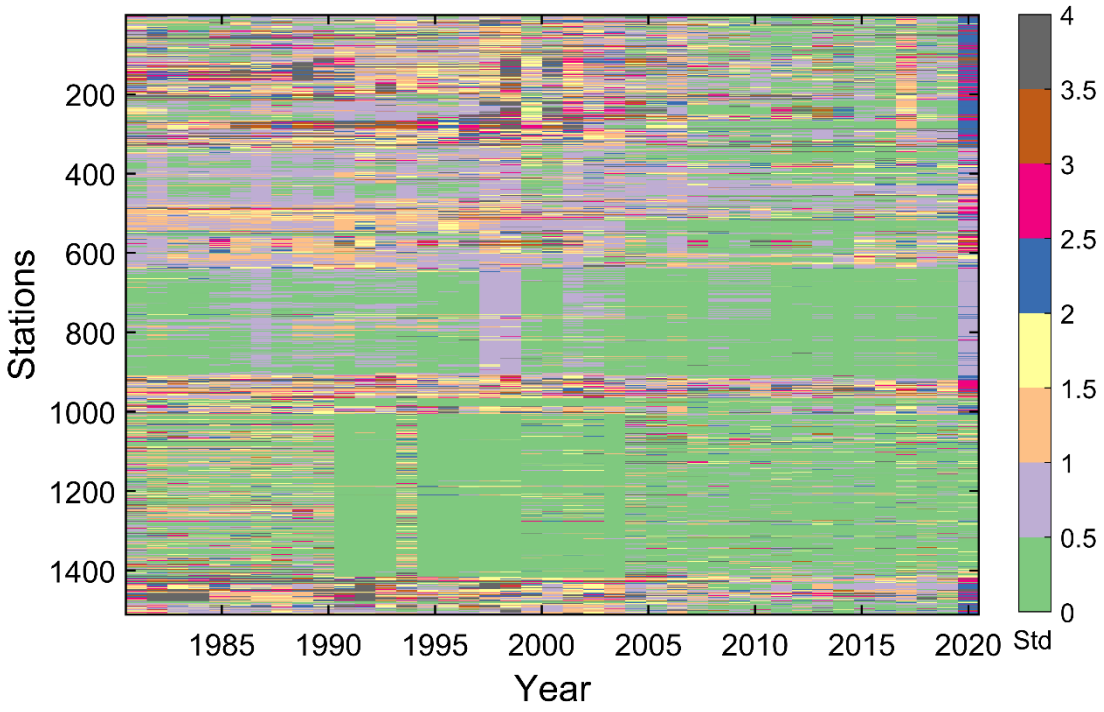

Appendix Figure A2. Standard deviation (Std) of daily observation (reporting) intervals across stations and years. The Std of the number of observations per day was greater than one for about 40% of the stations. Stations with irregular observation times tend to have larger std, for example, stations from 1400 to 1511 at the y-axis have different observation times year by year, so the std is generally larger than 1 time in each year.

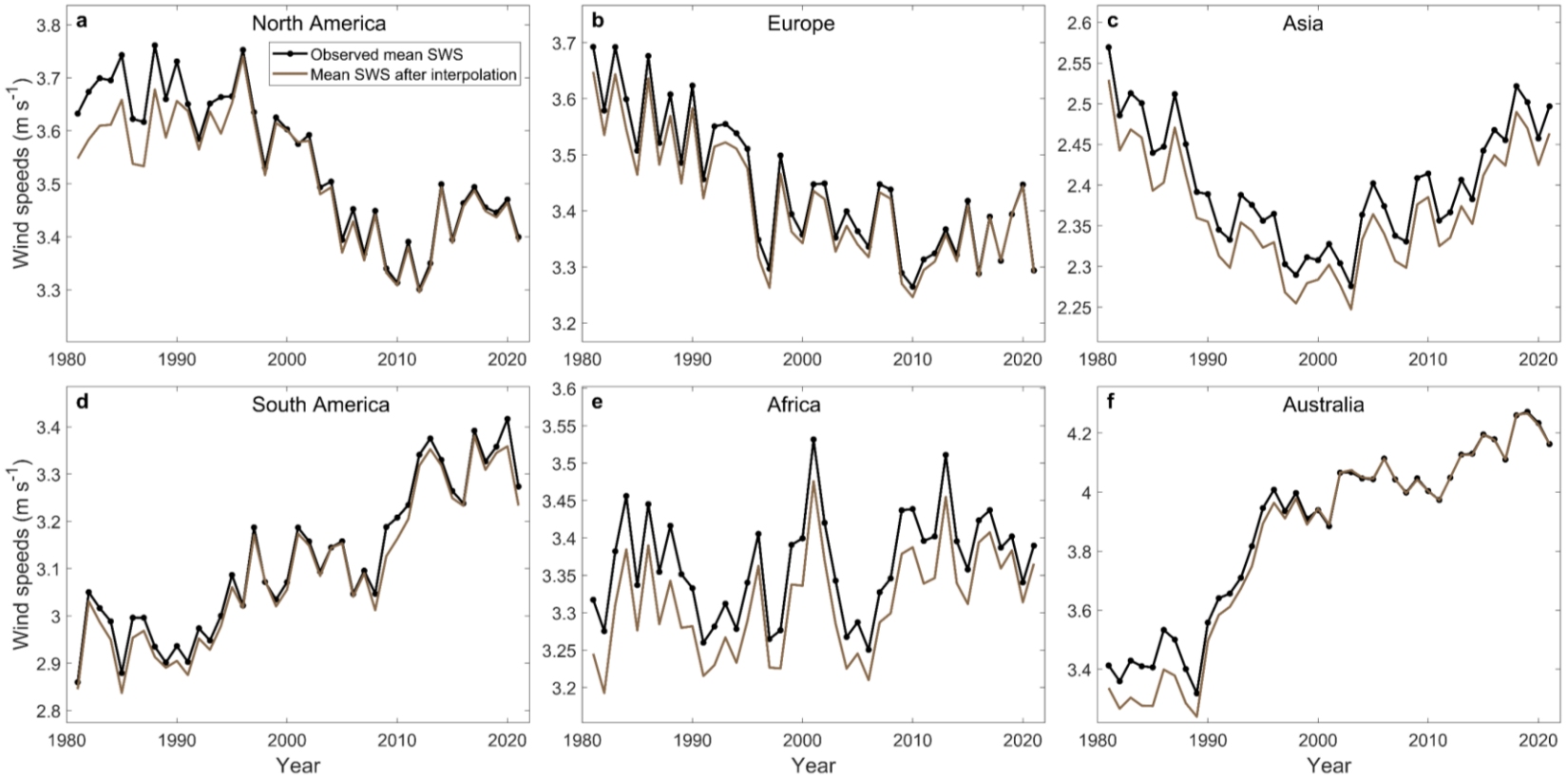

Appendix Figure A3. The comparison of continental average SWS between observed data and data after resampling. The black line is the mean SWS from observed data and the grown line is the mean SWS after resampling the time series. There are slight differences in the first decade of the observation time series and almost no difference during the reversal period in North America, Europe, South America and Australia. The bias always exists in Asia and Africa because the observation duration is still almost 3 hours in recent ten years.

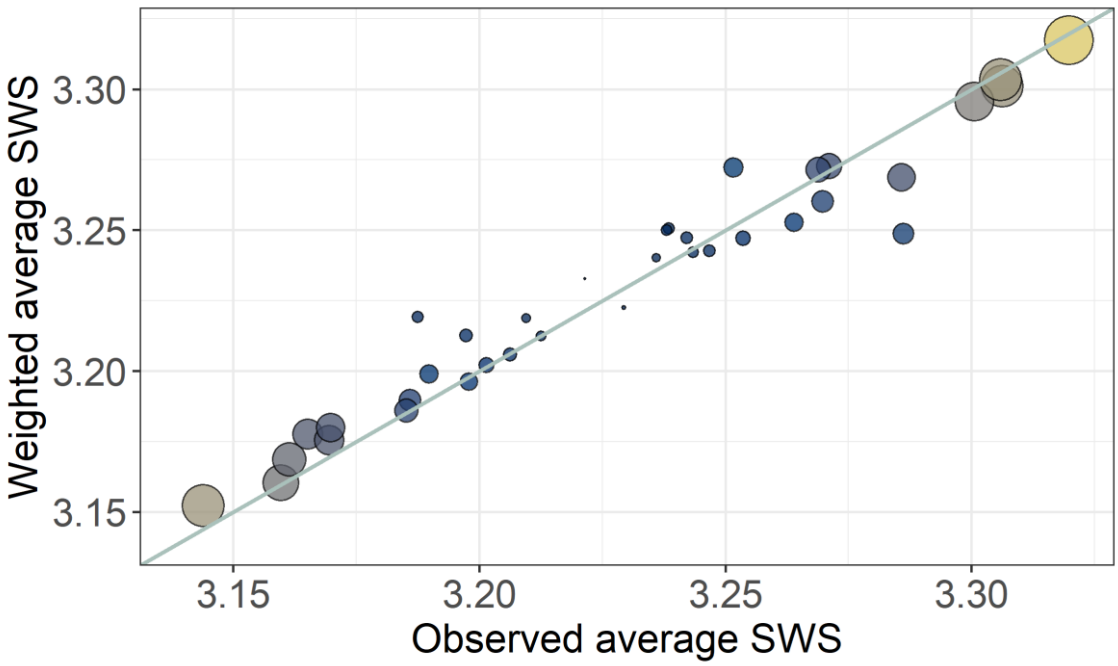

Appendix Figure A4. Scatter plot of weighted average SWS versus observed average SWS. The scatter plot shows the correlation between observed average SWS and weighted-average SWS. The size and color of each scatter represent the single coefficient of covariance. Weighted-average SWS is smaller than the observed average SWS overall, but still shows a great correlation with a Pearson correlation coefficient of 0.998 ($p < 0.05$).

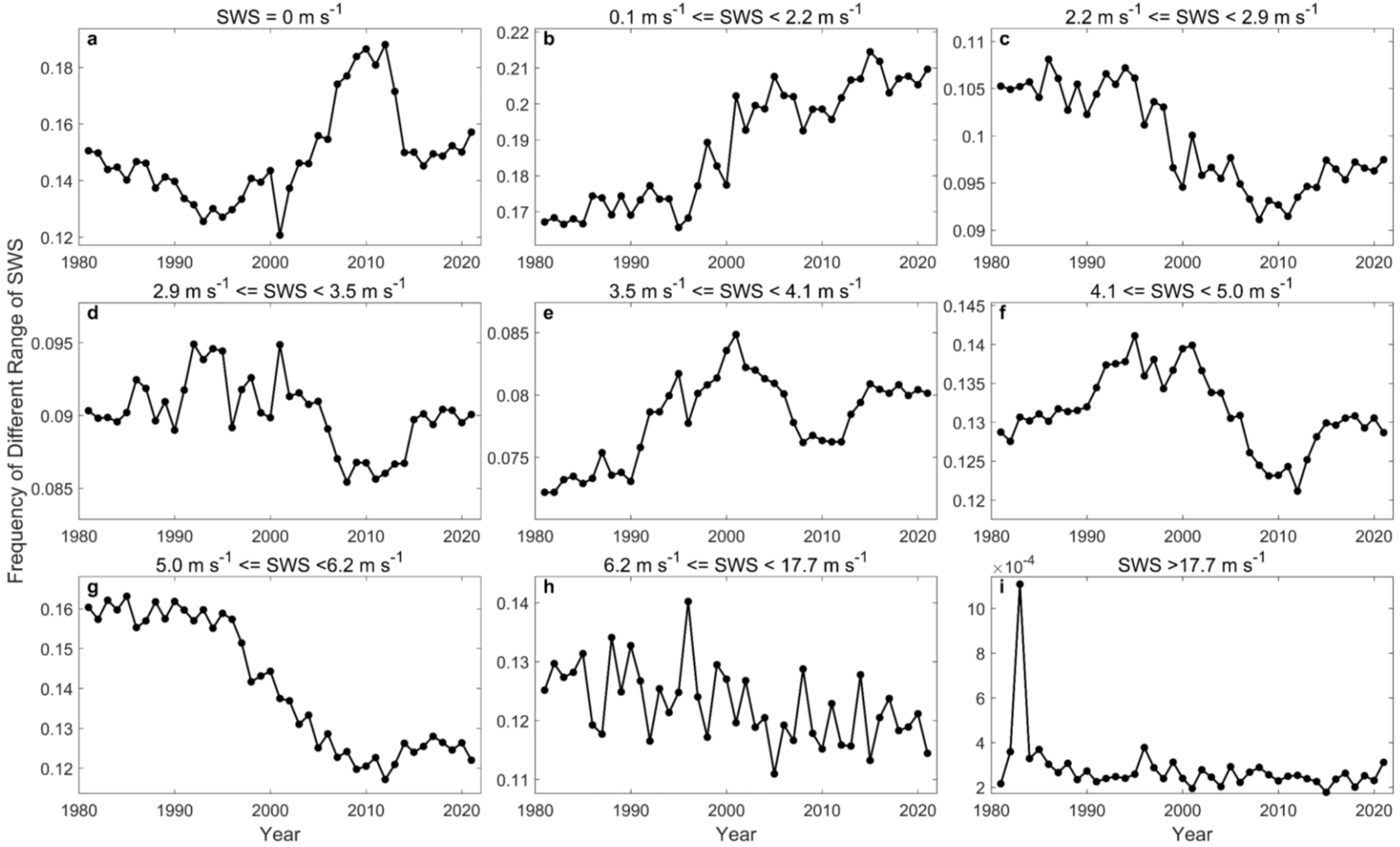

Appendix Figure A5. Frequency changes in North America. a-i) The frequency of SWS in America at specific classes.

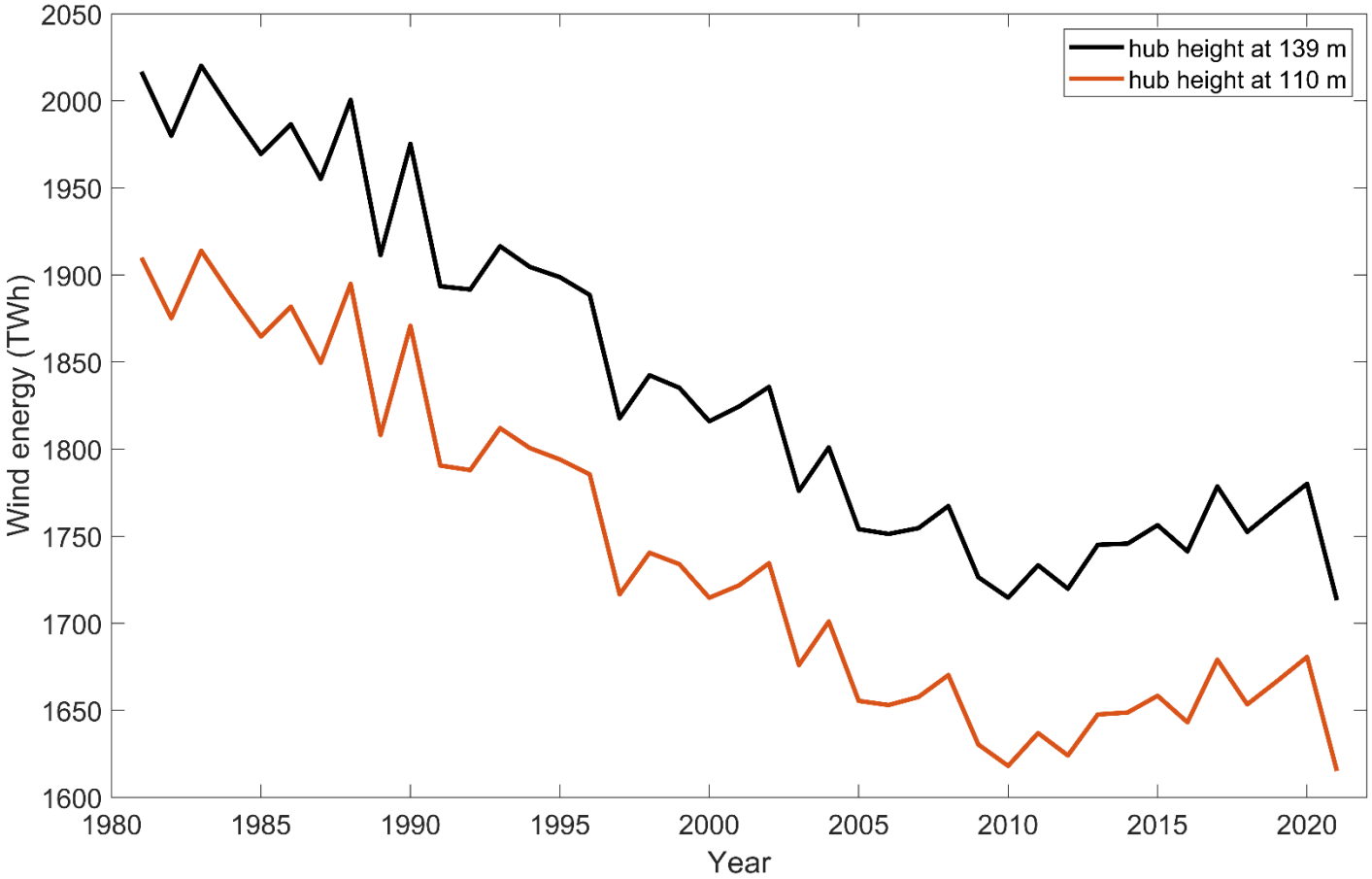

Appendix Figure A6: Wind energy of two hub heights. By assuming wind turbine GE 2.5-120 installed around observation stations at hub heights 139 m and 110m, wind energy is calculated based on the wind power curve and global wind power capacity (837 GW). Wind energy at hub height = 139 m is generally larger by 100 TWh than that at hub height = 110 m, with a very similar trend.